Editors' Suggestion | Featured in Physics

Odd-Even Parity of Nonlinear Hall Effects in Bilayer Graphene

Zitian Pan,[1,2,*] Jiaheng Li,[1,*] Jin Cao,[3] Xuejin Zhang,[3] Jundong Zhu,[1,2] Yu Hong,[1,2] Zhiheng Huang,[1,2] Jingwei Dong,[1,2] Dongxia Shi,[1,2] Kenji Watanabe,[4] Takashi Taniguchi,[5] Wei Yang,[1,2] Cong Xiao,[6] Shengyuan A. Yang,[3,†] Hongming Weng,[1,2,‡] Luojun Du,[1,2,§] and Guangyu Zhang[1,2,‖]

[1]*Beijing National Laboratory for Condensed Matter Physics and Institute of Physics, Chinese Academy of Sciences, Beijing 100190, China*

[2]*School of Physical Sciences, University of Chinese Academy of Sciences, Beijing 100190, China*

[3]*Research Laboratory for Quantum Materials, Department of Physics and Materials, The Hong Kong Polytechnic University, Kowloon, Hong Kong, China*

[4]*Research Center for Functional Materials, National Institute for Materials Science, 1-1 Namiki, Tsukuba 305-0044, Japan*

[5]*International Center for Materials Nanoarchitectonics, National Institute for Materials Science, 1-1 Namiki, Tsukuba 305-0044, Japan*

[6]*Interdisciplinary Center for Theoretical Physics and Information Sciences (ICTPIS), Fudan University, Shanghai 200433, China*

(Received 9 March 2026; revised 30 June 2026; accepted 8 September 2026; published 29 October 2026)

Odd-even effects are a generic feature of nonlinear physics, as odd- and even-order responses obey distinct symmetry conditions and reflect different aspects of electronic quantum geometry. With profound implications for both fundamental science and transformative applications, nonlinear Hall effects (NLHEs) have garnered intense interest in recent years, yet their odd-even parity remains elusive. Here, we report the observation of NLHE odd-even effects in bilayer graphene by engineering symmetry breaking. We demonstrate that even-order NLHEs necessitate an out-of-plane electric field to break inversion symmetry, whereas odd-order NLHEs require a perpendicular magnetic field to break vertical mirror planes in bilayer graphene. Interestingly, upon applying an out-of-plane magnetic field, we observe a new contribution to even-order NLHEs that increases linearly with field strength. By contrast, the magnetocontribution to odd-order NLHEs is dominated by a higher-order cubic scaling in magnetic field strength. Furthermore, both even- and odd-order NLHEs are strongly enhanced by Landau level formation, and the broken-symmetry Landau levels at filling factors $\nu = \pm 1, \pm 2$ can be clearly distinguished in the NLHE signals. These findings highlight that NLHEs are more sensitive to geometric and topological properties (e.g., Berry curvature hotspots) and symmetry breaking states than linear transport. Our work reveals the odd-even effects of NLHEs in bilayer graphene as well as electric and magnetic control of NLHEs with previously unexplored magnetocontributions, deepening the fundamental understanding of nonlinear transport and opening pathways toward technological advances in nonlinear electronics.

DOI: 10.1103/3x42-zb9r

Nonlinear effects offer powerful probes of the physical properties of materials beyond the linear responses, and constitute one of the most important research domains within condensed-matter physics, modern optics, and materials science [1–6]. In addition to the widely studied nonlinear optics, recent advances have opened a new branch of nonlinear physics, i.e., the emergent nonlinear electrical transport such as nonlinear Hall effect (NLHE) [3–5,7–19]. Notably, nonlinear transport can go beyond the constraint of linear charge transport and presents novel avenues to probe various quantum geometric properties of Bloch electrons. For example, by employing second- and third-order NLHEs, nontrivial band geometric and topological features, which are not accessible by linear transport, such as Berry-connection polarizability, Berry curvature dipoles, quadrupoles, and quantum metrics [13,14,16–18,20–38], have been demystified. Nonlinear electrical transport also opens up extraordinary opportunities to transform the landscape of a wide range of technological applications, e.g., Néel vector detection, wireless microwave detection, high-frequency rectification, topological memory, superconducting diodes, and energy-harvesting devices [12,24,32–34,39–47].

Nonlinear responses typically exhibit odd-even effects, as odd- and even-order nonlinear effects are fundamentally rooted in distinct symmetry breaking and usually involve different material properties [2,6,48,49]. For instance, in nonlinear optics, it is well known that even-order harmonic generations in the electric dipole approximation necessitate the breaking of inversion symmetry, whereas their

*These authors contributed equally to this work.
†Contact author: shengyuan.yang@polyu.edu.hk
‡Contact author: hmweng@iphy.ac.cn
§Contact author: luojun.du@iphy.ac.cn
‖Contact author: gyzhang@iphy.ac.cn

 © 2026 American Physical Society

odd-order counterparts do not [48–51]. One may naturally ask whether a similar phenomenon also occurs in nonlinear transport. In this Letter, we demonstrate the odd-even effects of NLHEs in a bilayer graphene system by engineering symmetry breaking. Breaking inversion symmetry by an out-of-plane gate electric field generates even-order NLHEs, whereas odd-order NLHEs requires a perpendicular magnetic field (B) to break the vertical mirror planes of bilayer graphene. Notably, applying a magnetic field induces new linear-in-B contributions to even-order NLHEs. By contrast, odd-order NLHEs are dominated by a higher-order magnetocontribution with cubic scaling in B. Furthermore, we find that NLHEs are strongly enhanced by the Landau level formation, with the broken-symmetry Landau levels of $\nu = \pm 1, \pm 2$ clearly distinguishable in the NLHE signals, implying a strong influence of Landau quantization and interaction effects on nonlinear transport.

Electric control of even-order NLHEs—High-quality, hexagonal boron nitride (h-BN) encapsulated dual-gate bilayer graphene devices are fabricated by a dry layer-by-layer transfer-and-stack technique (see Supplemental Material [52]). Figure 1(a) illustrates schematically the device structure. Few-layer graphene (Au) is used as the bottom (top) gate electrode to independently tune the carrier density (n) and out-of-plane displacement field (D). Notably, D can engineer the inversion symmetry breaking of bilayer graphene, which is required for even-order nonlinear effects. In experiment, the mth-order NLHEs are measured using a standard lock-in technique [Fig. 1(b)], where an ac driving current $I^{\omega} = I\sin(\omega t)$ with oscillating frequency ω is applied and the transverse Hall voltages $V_H^{m\omega}$ at harmonic frequencies $m\omega$ are recorded (Supplemental Material [52]).

Figure 1(c) presents the second- to fifth-order NLHEs measured under zero magnetic field and a displacement field of $D = 40$ mV/nm. Importantly, prominent even-order NLHEs including second- and fourth-order responses, are observed. By contrast, odd-order NLHEs, i.e., the third- and fifth-order effects, are negligible. This indicates that even- and odd-order NLHEs are constrained

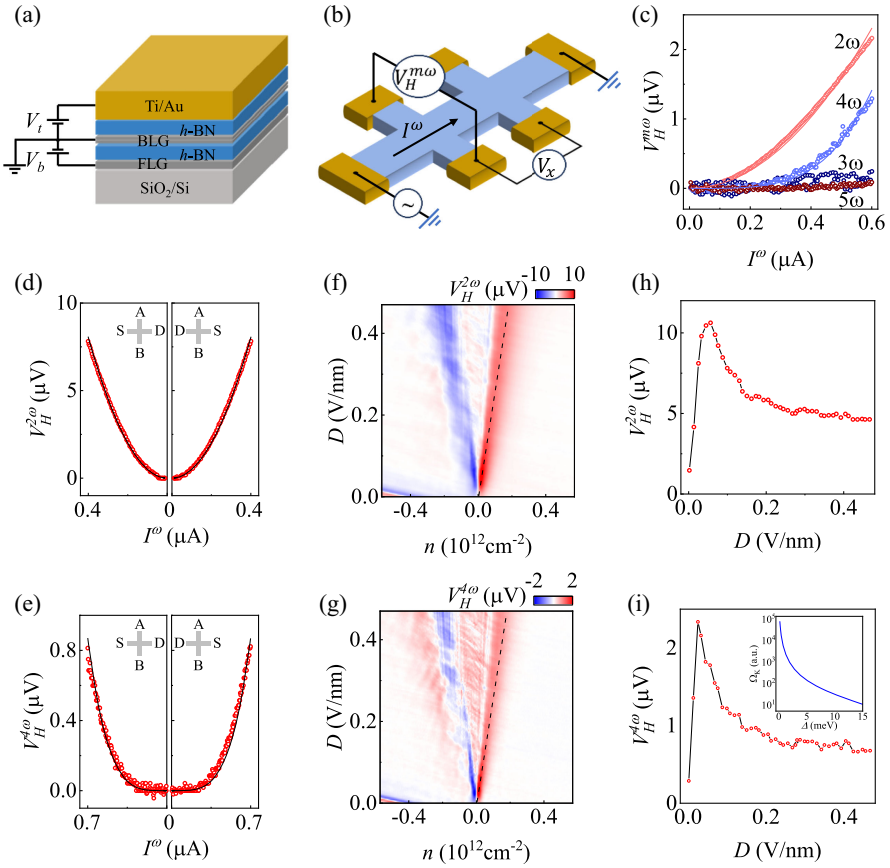


FIG. 1. Electric control of even-order NLHEs. (a) Schematic of h-BN encapsulated dual-gate bilayer graphene device (BLG, bilayer graphene; FLG, few-layer graphene). (b) Schematic of NLHE measurement in a Hall bar structure. (c) NLHE responses versus driving currents under $D = 40$ mV/nm and zero B. $V_H^{2\omega}$ has been divided by a factor of 10. (d),(e) $V_H^{2\omega}$ (d) and $V_H^{4\omega}$ (e) as a function of driving currents. Solid lines are quadratic (d) and quartic fitting (e). The insets show the electrode geometry for measurements. The current is injected from the S to D electrodes and the voltage is measured between the A and B electrodes. (f),(g) Color maps of $V_H^{2\omega}$ (f) and $V_H^{4\omega}$ (g) against D and n. (h),(i) $V_H^{2\omega}$ (h) and $V_H^{4\omega}$ (i) versus D. Inset: Berry curvature as a function of the energy gap Δ.

by different symmetry breakings, in resemblance to nonlinear optics [48,49]. $V_H^{2\omega}$ ($V_H^{4\omega}$) exhibits a parabolic (quartic) dependence on the excitation currents, and retains its sign upon reversal of the driving current direction [Figs. 1(d) and 1(e)], confirming the intrinsic even-order nonlinear nature [1,48,49]. It is noteworthy that potential measurement artifacts, e.g., spurious capacitive coupling, Schottky diode effects, and misalignments of the Hall bar arms, are precluded by the driving frequency-independent responses, linear dependence on I of linear longitudinal voltage V_x^{ω}, and negligible linear Hall response V_H^{ω} (Supplemental Material, Fig. 1 [52]). Figures 1(f) and 1(g), respectively, plot the color maps of second- and fourth-order NLHEs against D and n. Intriguingly, both $V_H^{2\omega}$ and $V_H^{4\omega}$ show pronounced peaks near the band edges (dashed lines, corroborated by linear longitudinal resistance mapping, Supplemental Material, Fig. 2 [52]) and switch their sign between hole and electron sides. Figures 1(h) and 1(i) display the evolution of $V_H^{2\omega}$ and $V_H^{4\omega}$ with D, respectively. Notably, $V_H^{2\omega}$ and $V_H^{4\omega}$ show a nonmonotonic dependence on D: they are nearly zero at $D = 0$, and exhibit a rapid rise followed by a decline with increasing D.

The above experimental observations demonstrate the electrically controlled even-order NLHE responses in bilayer graphene. At $D = 0$, inversion symmetry is preserved in bilayer graphene, thus forbidding any even-order NLHEs [1,48,49]. Upon applying a finite D, the inversion symmetry of bilayer graphene is broken, generating even-order NLHEs (please refer to symmetry analysis in Supplemental Material [52]). Notably, for bilayer graphene, the gate electric field opens a band gap proportional to D at K and K′ points, resulting in strong Berry curvature hotspots at the band edges (Supplemental Material, Fig. 3 [52]). Since Berry curvature underlies the chiral motion of Bloch electrons as well as the chiral scattering contributions such as side jump and skew scattering [21,39,45], this feature explains the strong response peaks near the band edges observed in Figs. 1(f) and 1(g). As for the nonmonotonic dependence of NLHEs on D, it can be understood by considering the following two competing factors. First, since the even-order NLHEs require finite D to break inversion symmetry, the NLHE signals should increase with D around $D = 0$. Second, it is known that the magnitude of Berry curvature would decrease with the band gap, i.e., with the increase of D [inset of Fig. 1(i)]. The competition between these two factors explains the nonmonotonic trend in Figs. 1(h) and 1(i).

Magnetic control of even-order NLHEs—Beyond the electric control of NLHEs, magnetic fields also offer opportunities to engineer NLHEs. Figure 2(a) plots the color map of $V_H^{2\omega}$ against B and n (please refer to the corresponding line slices in Supplemental Material, Figs. 4 and 5 [52]). Unless otherwise specified, the magnetic field is applied in the out-of-plane direction. Intriguingly, two prominent features are observed. First, $V_H^{2\omega}$ shows a Landau-fan-like feature and is strongly enhanced by triggering the formation of Landau levels (highlighted by dotted lines). Moreover, broken-symmetry Landau levels of

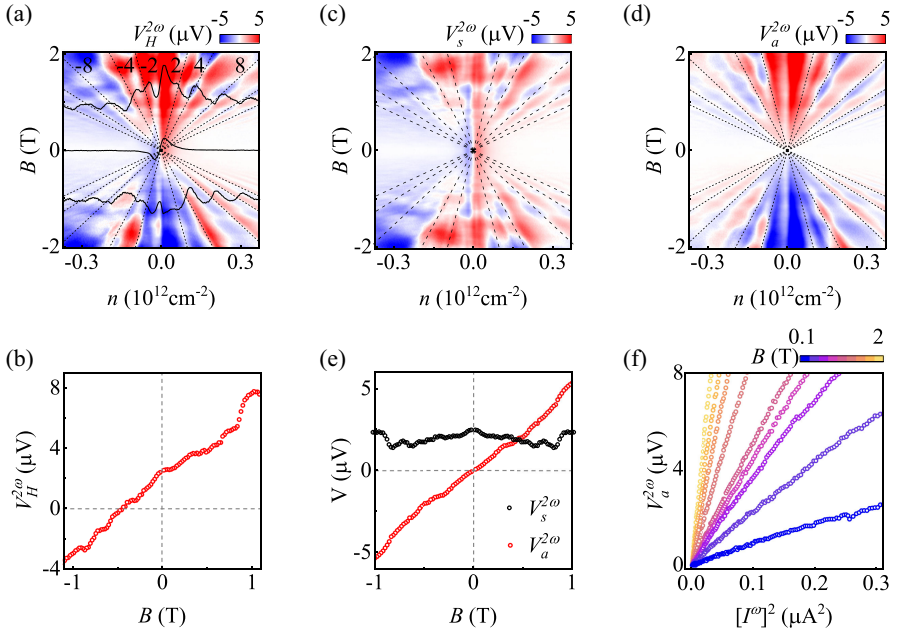


FIG. 2. Magnetic control of even-order NLHEs. (a) Color maps of $V_H^{2\omega}$ as a function of B and n measured at $I = 200$ nA and $D = 40$ mV/nm. Solid lines are line cuts at $B = 0, \pm 1$ T. Dashed lines track the Landau levels. (b) B-dependent $V_H^{2\omega}$. (c),(d) Color maps of $V_s^{2\omega}$ (c) and $V_a^{2\omega}$ (d) as a function of B and n. (e) $V_s^{2\omega}$ (black) and $V_a^{2\omega}$ (red) versus B. (f) $V_a^{2\omega}$ as a function of the square of driving currents.

$\nu = \pm 2$ are clearly distinguishable in $V_H^{2\omega}$, yet absent in the linear Hall and longitudinal resistance responses (Supplemental Material, Fig. 6 [52]). Note that the dashed lines marking the Landau levels are determined from the n-B diagram according to the Streda formula $\nu = (h/e)[1/(\partial B/\partial n)]$ [63]. Normally, in a noninteracting bilayer graphene, the sequence of filling factors is given by $\nu = \pm 4N$, and values observed beyond these are often signal of broken-symmetry states [64,65]. Our observation here suggests that NLHEs are more susceptible to Landau level formation and offers a more sensitive probe of broken-symmetry states. It is noteworthy that $V_H^{2\omega}$ scales quadratically with driving currents under all magnetic field conditions, consistent with the nature of second-order NLHE (Supplemental Material, Fig. 7 [52]). Second, near the neutral Dirac point and under relatively low B (< 1 T), where Landau levels do not form, $V_H^{2\omega}$ exhibits a linear dependence on B with a nonzero intercept [Fig. 2(b)]. This suggests that $V_H^{2\omega}$ contains two contributions and can be phenomenologically described as $V_H^{2\omega} = \alpha^{2\omega}[I^\omega]^2 + \beta^{2\omega}[I^\omega]^2 B$. The former B-independent term corresponds to conventional contributions discussed above in Fig. 1, while the latter, which scales linearly with B, accounts for a new contribution. To extract the B-independent and B-dependent terms, symmetric and antisymmetric operations are performed: $V_s^{2\omega} = \frac{1}{2}[V_H^{2\omega}(B) + V_H^{2\omega}(-B)] = \alpha^{2\omega}[I^\omega]^2$ and $V_a^{2\omega} = \frac{1}{2}[V_H^{2\omega}(B) - V_H^{2\omega}(-B)] = \beta^{2\omega}[I^\omega]^2 B$. Figures 2(c) and 2(d) plot, respectively, the color map of $V_s^{2\omega}$ and $V_a^{2\omega}$ against B and n. Near neutral Dirac points and under low B, $V_s^{2\omega}$ remains nearly unchanged, while $V_a^{2\omega}$ increases linearly with B [Fig. 2(e)]. Notably, the newly identified magneto-NLHE contribution $V_a^{2\omega}$ exhibits a linear scaling with the square of excitation currents across all magnetic fields [Fig. 2(f)], confirming the intrinsic second-order nonlinear nature.

The analogous B-induced behavior is also found for fourth-order NLHE, such as signal enhancement triggered by Landau level formation and the new contribution scaling linearly with B (Supplemental Material, Fig. 8 [52]). Interestingly, additional broken-symmetry states at $\nu = \pm 1$ are observed for fourth-order NLHE, underscoring that higher-order NLHEs may be more susceptible to broken-symmetry states and the underlying properties of a material.

Magnetic control of odd-order NLHEs—As noted in Fig. 1(c), odd-order NLHEs, in contrast to even-order ones, are suppressed in bilayer graphene in the absence of magnetic fields even under nonzero gate electric fields. This is a consequence of the crystal symmetry of bilayer graphene. Without D, bilayer graphene (Bernal stacking) has a point group of D_{3d}. Under an applied D, the inversion symmetry is broken, and the point group is reduced to C_{3v}, consisting of threefold rotational symmetry and three vertical mirror planes. This symmetry, however, still forbids the odd-order NLHEs, such as $V_H^{3\omega}$ and $V_H^{5\omega}$ studied here. By breaking the vertical mirror planes, an out-of-plane magnetic field can induce odd-order NLHEs in bilayer graphene (please refer to detailed symmetry analysis in Supplemental Material [52]). This expectation is confirmed by our experiment. Figure 3(a) shows the

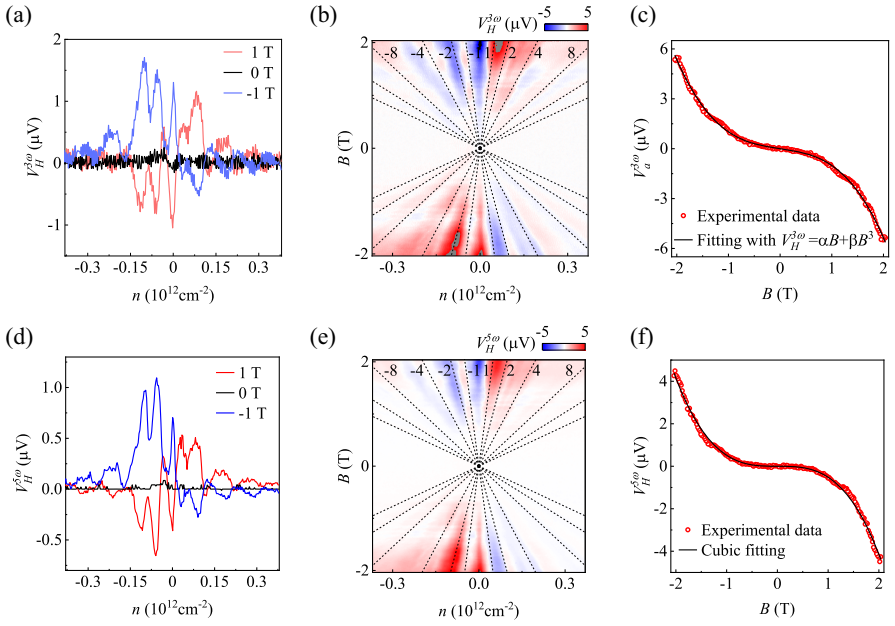


FIG. 3. Magnetic control of odd-order NLHEs. (a) $V_H^{3\omega}$ as a function of n at $B = 0, \pm 1$ T. (b) Color map of $V_H^{3\omega}$ against B and n measured at $I = 200$ nA and $D = 40$ mV/nm. Dashed lines track the Landau levels. (c) $V_H^{3\omega}$ as a function of B. Black line is the fitting result, where $\alpha = -0.458$ μV/T, $\beta = -0.555$ μV/T^3. (d) $V_H^{5\omega}$ as a function of n at $B = 0, \pm 1$ T. (e) Color map of $V_H^{5\omega}$ against B and n measured at $I = 400$ nA and $D = 40$ mV/nm. (f) $V_H^{5\omega}$ as a function of B. Black line is the cubic fitting result.

third-order NLHE response $V_H^{3\omega}$ under out-of-plane fields $B = 0, \pm 1$ T. One can see nonvanishing $V_H^{3\omega}$ emerges and exhibits opposite signs for positive and negative B. Figure 3(b) presents a color map of $V_H^{3\omega}$ as a function of B and n. In close resemblance to even-order NLHEs, the third-order NLHE responses are strongly enhanced by triggering Landau level formation, with broken-symmetry states observed at $\nu = \pm 1, \pm 2$. $V_H^{3\omega}$ exhibits a cubic dependence on the driving electric fields (Supplemental Material, Fig. 9 [52]), confirming its third-order nonlinear nature. Figure 3(c) shows the B dependence of $V_H^{3\omega}$. In stark contrast to the linear B dependence of $V_H^{2\omega}$ and $V_H^{4\omega}$, $V_H^{3\omega}$ exhibits pronounced nonlinearity, thus indicating high-order effect with respect to B. By carefully examining the data, we find that $V_H^{3\omega}$ can be fitted well by $V_H^{3\omega} = \alpha^{3\omega}[I^{\omega}]^3 B + \beta^{3\omega}[I^{\omega}]^3 B^3$ [black line, Fig. 3(c)]. To our best knowledge, such unusual B^3 behavior represents a hitherto unexplored effect in NLHEs and has not been reported before.

Furthermore, we underscore that analogous B-controlled characteristics are also observed for fifth-order NLHEs, encompassing a B^3 dependence and response enhancement driven by Landau level formation (Figs. 3(d)–3(f) and Supplemental Material, Fig. 10 [52]). We highlight that for fifth-order NLHE, $V_H^{5\omega}$ is almost entirely contributed by the B^3 component [black line, Fig. 3(f)], while the B-linear component is found to be negligible. Odd-order NLHEs driven by magnetic-field-induced symmetry breaking constitute a universal behavior applicable not only to bilayer graphene but also to a broad range of material systems. For example, by breaking time-reversal symmetry with an external magnetic field, odd-order NLHEs arising intrinsically from Berry curvature multipoles can emerge in nonmagnetic materials [36,66].

To clarify the underlying origin of B-induced NLHEs, we have performed scaling analysis. By carefully examining the scaling behavior, we find that $\sigma_a^{2\omega}/B$ can be perfectly fit by a quartic scaling relation $\sigma_a^{2\omega}/B \propto \sigma_x^4$, with negligibly small intercepts (Supplemental Material, Fig. 12 [52]). Such unconventional quartic scaling behavior is consistent with recent theoretical prediction as well as experimental observation, and suggests that Lorentz skew scattering, emerging from the interplay of classical Lorentz force and quantum skew scattering, may underpin the B-induced NLHEs [53–55]. For higher-order NLHEs, such as third-, fourth- and fifth-order NLHEs, although similar quartic scaling can also be observed (Supplemental Material, Fig. 13 [52]), the question of whether the mechanism is the same as that of the second-order NLHEs requires further theoretical calculations.

Conclusion—In conclusion, we demonstrate the odd-even effect of NLHEs in bilayer graphene through engineered symmetry breaking. Notably, even- and odd-order NLHEs are governed by distinct symmetry constraints: even-order NLHEs arise upon inversion symmetry breaking induced by out-of-plane electric fields, whereas odd-order NLHEs require magnetic-field-driven breaking of mirror-plane symmetry. The magnetocontribution to even-order NLHEs scales linearly with field strength, in contrast to odd-order NLHEs, which exhibit a previously unexplored higher-order response dominated by cubic scaling. Furthermore, both even- and odd-order NLHEs are strongly enhanced by Landau level formation, with broken-symmetry Landau levels at filling factors $\nu = \pm 1$, ± 2 clearly distinguishable in the NLHE signals. Our work demonstrates the NLHE odd-even effects and the feasibility of strong electric and magnetic control of NLHEs, while highlighting their potential as sensitive probes of broken-symmetry states and band geometry and topology (such as Berry curvature hotspots). These findings advance our understanding of NLHEs and open pathways toward transformative applications in low-dissipation rectifiers and efficient nonreciprocal devices.

Acknowledgments—This work is supported by the National Natural Science Foundation of China (NSFC, Grants No. 12422402, No. 61888102, No. 12274447, and No. 12574114), Beijing Natural Science Foundation (No. Z260002), the National Key R&D Program of China (Grants No. 2021YFA1202900 and No. 2023YFA1407000), the Strategic Priority Research Program of Chinese Academy of Sciences (No. XDB0470101), Quantum Science Strategic Special Project of Guangdong Province (No. GDZX2504003), HK PolyU start-up grant (No. P0057929), and the start-up funding from Fudan University.

L. D. and G. Z. supervised this work; L. D. and Z. P. conceived the project and designed the experiments; Z. P. fabricated the devices and carried out the electrical measurements; J. L. conducted the first principles calculations under the supervision of H. W.; J. C. and X. Z. performed symmetry analysis under the supervision of S. A. Y.; K. W. and T. T. provided high quality h-BN crystals; Z. P., L. D., C. X., and S. A. Y. analyzed the data; J. Z., Y. H., Z. H., J. D., D. S., and W. Y. helped with data analysis; Z. P., L. D., C. X., S. A. Y., J. L., and G. Z. cowrote the manuscript. All authors discussed the results and commented on the paper.

Data availability—There are no publicly available research data or software supporting this manuscript. Requests for further information or data should be sent to the authors.

[1] L. Du, Z. Huang, J. Zhang, F. Ye, Q. Dai, H. Deng, G. Zhang, and Z. Sun, Nat. Mater. **23**, 1179 (2024).
[2] J. Orenstein, J. E. Moore, T. Morimoto, D. H. Torchinsky, J. W. Harter, and D. Hsieh, Annu. Rev. Condens. Matter Phys. **12**, 247 (2021).

[3] Z. Z. Du, H.-Z. Lu, and X. C. Xie, Nat. Rev. Phys. **3**, 744 (2021).
[4] T. Ideue and Y. Iwasa, Annu. Rev. Condens. Matter Phys. **12**, 201 (2021).
[5] M. Suárez-Rodríguez, F. de Juan, I. Souza, M. Gobbi, F. Casanova, and L. E. Hueso, Nat. Mater. **24**, 1005 (2025).
[6] A. Autere, H. Jussila, Y. Dai, Y. Wang, H. Lipsanen, and Z. Sun, Adv. Mater. **30**, 1705963 (2018).
[7] I. Sodemann and L. Fu, Phys. Rev. Lett. **115**, 216806 (2015).
[8] T. Ideue, K. Hamamoto, S. Koshikawa, M. Ezawa, S. Shimizu, Y. Kaneko, Y. Tokura, N. Nagaosa, and Y. Iwasa, Nat. Phys. **13**, 578 (2017).
[9] Y. Tokura and N. Nagaosa, Nat. Commun. **9**, 3740 (2018).
[10] H. F. Legg *et al.*, Nat. Nanotechnol. **17**, 696 (2022).
[11] K. Yasuda, T. Morimoto, R. Yoshimi, M. Mogi, A. Tsukazaki, M. Kawamura, K. S. Takahashi, M. Kawasaki, N. Nagaosa, and Y. Tokura, Nat. Nanotechnol. **15**, 831 (2020).
[12] R. Wakatsuki, Y. Saito, S. Hoshino, Y. M. Itahashi, T. Ideue, M. Ezawa, Y. Iwasa, and N. Nagaosa, Sci. Adv. **3**, e1602390 (2017).
[13] K. Kang, T. Li, E. Sohn, J. Shan, and K. F. Mak, Nat. Mater. **18**, 324 (2019).
[14] Q. Ma *et al.*, Nature (London) **565**, 337 (2019).
[15] P. He, H. Isobe, G. K. W. Koon, J. Y. Tan, J. Hu, J. Li, N. Nagaosa, and J. Shen, Nat. Nanotechnol. **19**, 1460 (2024).
[16] J. Duan, Y. Jian, Y. Gao, H. Peng, J. Zhong, Q. Feng, J. Mao, and Y. Yao, Phys. Rev. Lett. **129**, 186801 (2022).
[17] Y. Gao, S. A. Yang, and Q. Niu, Phys. Rev. Lett. **112**, 166601 (2014).
[18] S. Lai *et al.*, Nat. Nanotechnol. **16**, 869 (2021).
[19] C. Xiao, J. Cao, Q. Niu, and S. A. Yang, Phys. Rev. Lett. **135**, 256306 (2025).
[20] P. He, H. Isobe, D. Zhu, C.-H. Hsu, L. Fu, and H. Yang, Nat. Commun. **12**, 698 (2021).
[21] P. Makushko *et al.*, Nat. Electron. **7**, 207 (2024).
[22] N. Wang *et al.*, Nature (London) **621**, 487 (2023).
[23] A. Gao *et al.*, Science **381**, 181 (2023).
[24] S. Sinha *et al.*, Nat. Phys. **18**, 765 (2022).
[25] X.-G. Ye, H. Liu, P.-F. Zhu, W.-Z. Xu, S. A. Yang, N. Shang, K. Liu, and Z.-M. Liao, Phys. Rev. Lett. **130**, 016301 (2023).
[26] X.-G. Ye, P.-F. Zhu, W.-Z. Xu, Z. Zang, Y. Ye, and Z.-M. Liao, Phys. Rev. B **106**, 045414 (2022).
[27] M. Huang *et al.*, Phys. Rev. Lett. **131**, 066301 (2023).
[28] H. Li, C. Zhang, C. Zhou, C. Ma, X. Lei, Zijing Jin, H. He, B. Li, K. Tuen Law, and J. Wang, Nat. Commun. **15**, 7779 (2024).
[29] X.-Y. Liu, A.-Q. Wang, D. Li, T.-Y. Zhao, X. Liao, and Z.-M. Liao, Phys. Rev. Lett. **134**, 026305 (2025).
[30] M.-S. Qin, P.-F. Zhu, X.-G. Ye, W.-Z. Xu, Z.-H. Song, J. Liang, K. Liu, and Z.-M. Liao, Chin. Phys. Lett. **38**, 017301 (2021).
[31] T. Ahmed, B. Q. Tu, K. Watanabe, T. Taniguchi, M. Gobbi, F. Casanova, and L. E. Hueso, ACS Nano **19**, 24930 (2025).
[32] M. Suárez-Rodríguez *et al.*, Phys. Rev. Lett. **132**, 046303 (2024).
[33] H. Liu, J. Zhao, Y.-X. Huang, W. Wu, X.-L. Sheng, C. Xiao, and S. A. Yang, Phys. Rev. Lett. **127**, 277202 (2021).
[34] C. Wang, Y. Gao, and D. Xiao, Phys. Rev. Lett. **127**, 277201 (2021).
[35] H. Liu, J. Zhao, Y.-X. Huang, X. Feng, C. Xiao, W. Wu, S. Lai, W. B. Gao, and S. A. Yang, Phys. Rev. B **105**, 045118 (2022).
[36] C.-P. Zhang, X.-J. Gao, Y.-M. Xie, H. C. Po, and K. T. Law, Phys. Rev. B **107**, 115142 (2023).
[37] F. Wu *et al.*, Phys. Rev. Lett. **131**, 256201 (2023).
[38] J. Zhao *et al.*, Nature (London) **639**, 354 (2025).
[39] H. Isobe, S.-Y. Xu, and L. Fu, Sci. Adv. **6**, eaay2497 (2020).
[40] J. Godinho *et al.*, Nat. Commun. **9**, 4686 (2018).
[41] D. Kumar, C.-H. Hsu, R. Sharma, T.-R. Chang, P. Yu, J. Wang, G. Eda, G. Liang, and H. Yang, Nat. Nanotechnol. **16**, 421 (2021).
[42] Y. Zhang and L. Fu, Proc. Natl. Acad. Sci. U.S.A. **118**, e2100736118 (2021).
[43] L. Min *et al.*, Nat. Commun. **14**, 364 (2023).
[44] X. F. Lu, C.-P. Zhang, N. Wang, D. Zhao, X. Zhou, W. Gao, X. H. Chen, K. T. Law, and K. P. Loh, Nat. Commun. **15**, 245 (2024).
[45] P. He, G. K. W. Koon, H. Isobe, J. Y. Tan, J. Hu, A. H. C. Neto, L. Fu, and H. Yang, Nat. Nanotechnol. **17**, 378 (2022).
[46] B. Cheng, Y. Gao, Z. Zheng, S. Chen, Z. Liu, L. Zhang, Q. Zhu, H. Li, L. Li, and C. Zeng, Nat. Commun. **15**, 5513 (2024).
[47] A. Tiwari *et al.*, Nat. Commun. **12**, 2049 (2021).
[48] Y.-R. Shen, *Principles of Nonlinear Optics* (Wiley, Hoboken, 2002).
[49] R. W. Boyd, *Nonlinear Optics* (Academic Press, New York, 2020).
[50] W. Jin, E. Drueke, S. Li, A. Admasu, R. Owen, M. Day, K. Sun, S.-W. Cheong, and L. Zhao, Nat. Phys. **16**, 42 (2020).
[51] X. Luo, D. Obeysekera, C. Won, S. H. Sung, N. Schnitzer, R. Hovden, S.-W. Cheong, J. Yang, K. Sun, and L. Zhao, Phys. Rev. Lett. **127**, 126401 (2021).
[52] See Supplemental Material at http://link.aps.org/supplemental/10.1103/3x42-zb9r for additional information about the device fabrication, symmetry-constrained NLHEs, the intrinsic nature of the NLHE response, electrically tunable Berry curvature in bilayer graphene, linear magnetotransport, extended data for magnetic control of NLHEs, and scaling analysis of NLHEs, which includes Refs. [13,21,39,49,53–62].
[53] C. Xiao, Y.-X. Huang, and S. A. Yang, Nat. Commun. **17**, 3632 (2026).
[54] X. F. Lu *et al.*, Nat. Commun. **17**, 6221 (2026).
[55] P. He *et al.*, arXiv:2511.03381v1.
[56] L. Xie, L. Du, X. Lu, R. Yang, D. Shi, and G. Zhang, Chin. Phys. B **26**, 087306 (2017).
[57] Z. Huang *et al.*, Nat. Commun. **15**, 4586 (2024).
[58] S. Iwakiri, L. V. Ginzburg, M. P. Röösli, Y. Meir, A. Stern, C. Reichl, M. Berl, W. Wegscheider, T. Ihn, and K. Ensslin, Phys. Rev. Res. **5**, L032046 (2023).
[59] J. Yin, C. Tan, D. Barcons-Ruiz, I. Torre, K. Watanabe, T. Taniguchi, J. C. W. Song, J. Hone, and F. H. L. Koppens, Science **375**, 1398 (2022).
[60] E. McCann and V. I. Fal'ko, Phys. Rev. Lett. **96**, 086805 (2006).

[61] D. Xiao, M.-C. Chang, and Q. Niu, Rev. Mod. Phys. **82**, 1959 (2010).
[62] K. S. Novoselov, E. McCann, S. V. Morozov, V. I. Fal'ko, M. I. Katsnelson, U. Zeitler, D. Jiang, F. Schedin, and A. K. Geim, Nat. Phys. **2**, 177 (2006).
[63] Y. Xie *et al.*, Nature (London) **600**, 439 (2021).
[64] B. E. Feldman, J. Martin, and A. Yacoby, Nat. Phys. **5**, 889 (2009).
[65] Y. Zhao, P. Cadden-Zimansky, Z. Jiang, and P. Kim, Phys. Rev. Lett. **104**, 066801 (2010).
[66] L. Du, T. Hasan, A. Castellanos-Gomez, G.-B. Liu, Y. Yao, C. N. Lau, and Z. Sun, Nat. Rev. Phys. **3**, 193 (2021).